JCTC Journal of Chemical Theory and Computation

First-Principle Molecular Dynamics Study of Selected Schiff and Mannich Bases: Application of Two-Dimensional Potential of Mean Force to Systems with Strong Intramolecular Hydrogen Bonds

Aneta Jezierska*,†,§ and Jarosław J. Panek‡

University of Wrocław, Faculty of Chemistry, F. Joliot-Curie 14, 50-383 Wrocław, Poland, and National Institute of Chemistry, Hajdrihova 19, 1001 Ljubljana, Slovenia

Received October 9, 2007

Abstract: Car−Parrinello Molecular Dynamics simulations were performed for selected anharmonic systems, i.e., Schiff and Mannich base-type compounds, to investigate the vibrational properties associated with O−H stretching. All calculations were performed in the gas phase to compare them with available experimental data. First the vibrational properties of the two compounds were analyzed on the basis of well-established approaches: Fourier transformation of the autocorrelation function of both the atomic velocities and dipole moments. Then path integral molecular dynamics simulations were performed to demonstrate the influence of quantum effects on the proton's position in the hydrogen bridge. In addition, quantum effects were incorporated a posteriori into calculations of O−H stretching envelopes for the Schiff and Mannich bases. Proton potential snapshots were extracted from the ab initio molecular dynamics trajectory. Vibrational Schrödinger equations (one- and two-dimensional) were solved numerically for the snapshots, and the O−H stretching envelopes were calculated as a superposition of the 0→1 transitions. Subsequently, one- and two-dimensional potentials of mean force (1D and 2D pmf) were calculated for the proton stretching mode from the proton vibrational eigenfunctions and eigenvalues incorporating statistical sampling and nuclear quantum effects. The results show that the applied methodologies are in good agreement with experimental infrared spectra. Additionally, it is demonstrated that the 2D pmf method could be applied in systems with strong anharmonicity to describe the properties of the O−H stretching mode more accurately. Future applications of the 2D pmf technique include, in principle, large biomolecular systems treated within the QM/MM framework.

I. Introduction

Intramolecular hydrogen-bonding plays a crucial role in biologically relevant systems and materials science, two important areas of contemporary research.[1−5] Its advantage over intermolecular interactions stems from the fact that the molecular scaffolding provides a rigid, durable framework for the weaker, modifiable hydrogen bridge of interest. The formation of an intramolecular hydrogen bond is entropically favorable over intermolecular contacts because of the formation of a pseudoring. Two examples of groups of compounds possessing strong intramolecular hydrogen bonds are aromatic Schiff and Mannich bases. The introduction of substituents either in the phenyl ring or at the acceptor

* Corresponding author phone: (+48) 71-3757-308; fax: (+48) 71-3282-348; e-mail: anetka@elrond.chem.uni.wroc.pl.

† University of Wrocław.

‡ National Institute of Chemistry.

§ Current address: The International School for Advanced Studies (SISSA), INFM DEMOCRITOS, Italian Institute of Technology- SISSA Unit, Via Beirut 2-4, 34014 Trieste, Italy.

10.1021/ct7002644 CCC: $40.75
Published on Web 02/12/2008

nitrogen atom leads to fine-tuning of the bridge properties[6−9] with direct influence on the macroscopic characteristics valuable for the practical application of the studied compounds. The main difference between the molecular skeletons of Schiff and Mannich bases is the presence of a double bond in the imine group, a hydrogen bond acceptor in the former class of compounds. The double bond enables coupling between the hydrogen bridge and the aromatic π-electron system of the phenyl ring. This in turn leads to a shortening of the bridge, which is classified as a low-barrier hydrogen bond (LBHB).[10] The flattening of the potential energy surface (PES) of the proton motion results in observable proton-transfer phenomena. The substitution in the phenyl ring or the imine group can influence the hydrogen bridge either by induction or steric effects.[11−13] Induction is a classical mechanism of electron withdrawal or electron donation, which is dependent on the electronic character of the substituents. On the other hand, a steric influence is provided by bulky substituents especially in the *ortho* position of the aromatic ring or in the imine group of both classes of these compounds. The microscopic results of the above effects are visible in the large variations of the hydrogen bridge's geometrical and spectroscopic parameters. The most significant are shifts observed in the vibrational, electronic, and NMR spectra.[14,15] The microscopically observed effects are related to and further responsible for the exhibited molecular properties important from the biological and industrial points of view. Schiff bases were found to be involved in the biological processes of vision and photoconversion.[16−21] Their potential practical applications are due to photochromic, thermochromic, magnetic, and conducting properties.[22−26] Mannich bases exhibit cytotoxic properties which lead to diverse biological activity found experimentally[27−31] and commercially exploited in, for example, derivatives of Norfloxacin (an antibiotic used to treat certain infections caused by bacteria—such as gonorrhea—and prostate and urinary tract infections).[32−34] They have found industrial application as lubricating oil additives[35] and epoxy resin hardeners.[36]

The current study discusses in detail the hydrogen bridge properties of the two model systems chosen from the Schiff and Mannich base families (Figure 1).[37,9] The selected Schiff base is N-methyl-2-hydroxybenzylidene amine (HBZA) and the representative Mannich base is *ortho*-dimethylaminomethylphenol (DMAP). Their structural similarity allows us to compare directly the molecular properties of the two classes of compounds with emphasis on the proton dynamics in the hydrogen bridge. The size of the studied molecules is small enough to allow a clear understanding of the proton dynamics and the exclusion of unwanted interactions. On the other hand, the models are sufficiently large to require statistical description via ab initio molecular dynamics.[38] Molecular dynamics provides a bridge between the microscopic and macroscopic levels of describing the studied systems. The potential energy surface obtained from first-principle methods (in our case, density functional theory, DFT,[39,40] propagated in time using the Car−Parrinello[38] scheme) allows us to study chemical reaction pathways such as the proton dynamics in the hydrogen bridge. Time evolution of the electronic and structural features gives us a more detailed description of the hydrogen bridge's properties. In particular, a set of frozen-nuclei proton potential functions can be converted into an ensemble-averaged free energy profile defined as the potential of mean force[41] for the proton motion. Using free energy profiles instead of static proton potential functions might be advantageous for describing processes involving large systems (e.g., enzymes), where the huge number of degrees of freedom prevents the use of only one representative total-energy profile. In the current study we extend the scheme for estimating the potential of mean force of the proton motion from the one-dimensional (1D pmf) to the two-dimensional (2D pmf) case. This helps us visualize the qualitative and quantitative differences in the molecular properties provided by the molecular frameworks of the Schiff and Mannich base. Our calculated results are verified by comparison with available experimental infrared (IR) spectra and previous theoretical investigations.[9,37] Summarizing, the main goal of our study is a description of the proton dynamics in two closely related molecular skeletons exhibiting short, strong, low-barrier (Schiff base) and medium-strong (Mannich base) intramolecular hydrogen bonds. The outline of the article is as follows: the theory and methods applied in the study are presented in section II, the results and discussion are given in section III, and concluding remarks are presented in section IV.

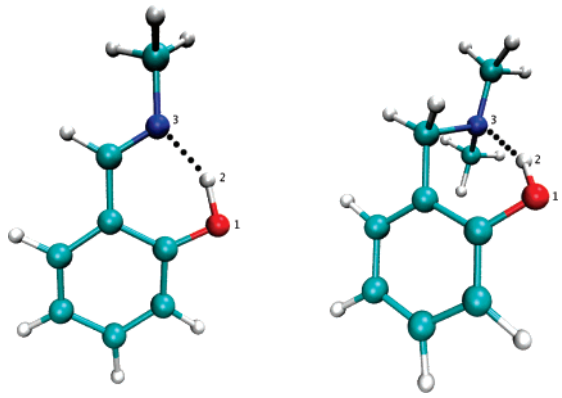

Figure 1. Computational models of the investigated Schiff (N-methyl-2-hydroxybenzylidene amine, HBZA) (left side) and Mannich (*ortho*-dimethylaminomethylphenol, DMAP) (right side) bases with the atom numbering scheme. Only selected atoms, important in the results discussion, are marked. Color coding of atoms is as follows: cyan − carbon; dark blue − nitrogen (atom 3); red − oxygen (atom 1); white − hydrogen.

II. Theory and Methods

A. Car−Parrinello Molecular Dynamics (CPMD) in Vacuo. Car−Parrinello Molecular Dynamics[38] (CPMD) on the basis of Density Functional Theory[39,40] (DFT) was applied to investigate vibrational features of the selected Schiff (N-methyl-2-hydroxybenzylidene amine, HBZA) and Mannich (*ortho*-dimethylaminomethylphenol, DMAP) bases (see Figure 1) in vacuo. The initial structure optimizations were carried out using the Schlegel Hessian matrix at the starting point.[42] The cubic cell dimension for both compounds was $a = 15$ Å. The size of the cell was dictated by the need to avoid artifacts at the cell boundary. The Hockney periodic

image removal scheme was applied. The functional proposed by J. P. Perdew, K. Burke, and M. Ernzerhof (PBE) in conjunction with the plane-wave basis set was used for the study.[43] The pseudopotentials proposed by Troullier and Martins[44] were used to replace the core electrons of the atoms in the system studied. A kinetic energy cutoff of 70 Ry was applied for the plane-wave basis set. The initial period of the molecular dynamics (ca. 10 000 steps) was used to equilibrate both studied systems and was not further analyzed or discussed. During the molecular dynamics (MD) simulations, the time step was consistently set to 3 au (0.0725 fs), and a fictitious electron mass parameter (EMASS) of 400 au was used to reproduce the orbital dynamics. The simulations were performed at room temperature ($T = 300$ K) for the Schiff base, and $T = 390$ K was used for the Mannich base. The data collection was 10.5 ps for the Schiff base and 12.5 ps for the Mannich base. Vibrational features of the two compounds were analyzed on the basis of the power spectra of the atomic velocities. In addition, the dipole moment values were collected during the MD run and were subsequently used to generate the predicted IR spectra. A program for Fourier transform autocorrelation function calculations was used for this purpose. The time evolution of the interatomic distances related to the intramolecular hydrogen bond was analyzed using programs developed in our laboratory.

B. Path Integral Molecular Dynamics (PIMD). Path Integral Molecular Dynamics[45−47] (PIMD) simulations were then carried out for the studied compounds in vacuo. PIMD was performed using a setup similar to the one applied for the CPMD simulations. The calculations were also performed at $T = 300$ K (for Schiff base) and $T = 390$ K (for Mannich base), controlled by a Nosé-Hoover thermostat chain.[48−51] Eight Trotter replicas ($P = 8$) were used for imaginary time path integration. The staging representation of the path integral propagator was applied.[52,47] The data were collected for 9 ps after an initial equilibration and further used to obtain a histogram presenting the hydrogen (H2) position in the intramolecular hydrogen bond.

C. A Posteriori Inclusion of Quantum Effects of Nuclear Motion into Calculation of the Vibrational Features of the Intramolecular Hydrogen Bond. The inclusion of quantum effects of the O−H stretching in the studied Schiff and Mannich bases was performed using an envelope methodology.[5] The method consists of a posteriori quantum corrections obtained by solving the vibrational Schrödinger equation[53] for a set of proton potential functions. These functions are obtained from the Car−Parrinello Molecular Dynamics trajectory of the investigated molecules sampled at regular intervals (0.2 ps). Such an interval, being ca. ten times larger than heavy atom vibrations, was chosen to minimize correlation between snapshots while providing sufficient number of structures. Regular, unbiased sampling of the CPMD trajectory, corresponding to the NVT ensemble by the virtue of Nosé-Hoover thermostat, ensures that the snapshots also closely follow the canonical statistical ensemble. Subsequently, the resulting snapshots are processed in the following way: the selected proton of the hydrogen bridge is displaced along a circular arc defined uniquely by the positions of the donor, proton, and acceptor atoms.[54] A total of 40 evenly spaced points are generated on this arc, and after rejecting those giving too close contact (less than 0.7 Å) with either donor or acceptor atom, 18 to 24 positions for a bridge proton are obtained for each snapshot. Then, the total energy is calculated for each frozen structure with the proton placed in the subsequent positions on the arc. Thus, for each snapshot, an instantaneous proton potential function is obtained which serves in solving the quantum vibrational problem with two-step methodology and software described in ref 53. First, the proton potential function is approximated by a ninth degree polynomial; the fit accuracy was usually better than 0.05 kcal/mol at each point. Second, the vibrational Schrödinger equation is solved using Fourier grid technique with 300 grid points evenly spaced in the range from 0.7 Å to 2.0 Å as a real-space basis set. This procedure yields vibrational energy levels and wavefunctions for each snapshot taken from the CPMD trajectory. The set of quantum-corrected anharmonic vibrational frequencies then serves finally to construct an envelope of the O−H stretching mode by summing a set of Gaussian functions centered at each of the calculated frequencies. This procedure has been previously successfully applied to a model structure (a Mannich base-type compound) with an intramolecular hydrogen bond.[55,56]

The dynamics simulations concerning parts A, B, and C above were performed using the CPMD v.3.9.2 program[57] compiled with parallel support to maximize the efficiency of the time-consuming calculations.

D. One- and Two-Dimensional Potentials of Mean Force (1D and 2D pmf). Finally, the one and two-dimensional potentials of mean force (1D and 2D pmf) were calculated for the O−H stretching mode on the basis of eigenfunctions obtained by solving the vibrational Schrödinger equation. The potential of mean force is a *free energy* profile along the postulated reaction coordinate.[41] Combined use of statistical sampling by Car−Parrinello molecular dynamics and quantization of the nuclear motions provides the following scheme of computing the pmf applied in this study. For each selected molecular dynamics snapshot, the 1D vibrational Schrödinger equation was solved, and the resulting eigenfunctions are stored (see previous subsection C). The squared wavefunction represents the probability density $\rho(x)$, where x is the chosen coordinate, in this case the O−H distance. In more detail, the probability density reads

$$\rho(x) = \frac{\sum_{i=0}^{\infty} \Psi_i^2(x) e^{-E_i/kT}}{\sum_{i=0}^{\infty} e^{-E_i/kT}}$$

where i runs over the vibrational eigenfunctions and eigenvalues.

The vibrational energy scale is assumed to be shifted so that the ground-state energy E_0 is 0 in the above formula. The main contribution to $\rho(x)$ comes from the ground vibrational state; the excited states contribute much less. However, in this study we chose to include contributions from the two lowest-lying excited states (i.e., $i = 0, 1, 2$) as well, since we observed large anharmonicity and correspond-

ingly flat potential energy surfaces in one of the studied systems (see below). Subsequently, the $\rho(x)$ is averaged over the molecular dynamics trajectory, and the pmf is calculated directly from the expression:

$$\mathrm{pmf}(x) = -k_B T \ln \langle \rho(x) \rangle$$

The probability density $\rho(x)$ is in this case a Boltzmann-averaged sum of the squared wavefunctions, and the angle brackets denote averaging over the molecular dynamics snapshots. The applied method for the pmf calculations directly incorporates the quantum nature of the proton motion.[55] Additionally, this procedure is based on the potential energy surface calculated using nonempirical electronic structure methods only. This fact provides some advantage in systems for which force-field parametrization would be difficult, such as metals, organometallics, etc. It should be noted that many elegant and successful methods of calculating the potential of mean force are based on the force-field approach, including studies of intramolecular hydrogen bonds[58] parametrized to the DFT potential energy surface. Detailed discussion of the pmf calculation method employed here—its applicability range and relation to other techniques—is given at the end of the Results and Discussion.

The extension of the one-dimensional pmf technique to the two-dimensional case was carried out by choosing two reaction coordinates significant for proton dynamics. The extraction of snapshots from the CPMD trajectory suggests the application of the clamped nuclei model, in which the donor−acceptor distance is fixed at the value present in a given trajectory frame. The two coordinates applied in our study are therefore the O−H distance (as in the 1D case) and the O−H...N angle. For each extracted frame, the bridge proton position was scanned along these two coordinates. The angle was set to a value ranging from 110° to 180° in 5° increments, and at each fixed value of the angle the proton was displaced along the arc defined analogously to the one-dimensional case. This approach assumes a semicylindrical symmetry of the proton potential surface with respect to the donor − acceptor axis. The assumption is reasonable in our small-molecule, gas-phase models by the lack of bulky groups or intermolecular contacts and provides significant reduction of computational effort with respect to the full 3D scan of proton potential function. The set of the DFT total energy values for the generated coordinates forms a grid on which the 2D vibrational Schrödinger equation is solved, using the computational approach described above in subsection C, but extended to two dimensions. The resulting eigenfunctions are then stored for final ensemble averaging, which yields the 2D pmf according to the formula

$$\mathrm{pmf}(x, y) = -k_B T \ln \left\langle \frac{\sum_{i=0}^{\infty} \Psi_i^2(x, y) e^{-E_i/kT}}{\sum_{i=0}^{\infty} e^{-E_i/kT}} \right\rangle$$

where x and y are the chosen internal coordinates.

Test calculations indicated that because of the smaller gaps between the eigenvalues in comparison with the 1D case, it is obligatory to include the eigenfunctions of the ground state and two subsequent excited states from the solution of the 2D vibrational problem during the pmf calculation. The one- and two-dimensional potentials of mean force (1D and 2D pmf) were calculated using programs written especially for the purpose of this project. The graphical representation of the obtained results was prepared using the VMD[59] and Gnuplot[60] programs.

Table 1. Average Values and Standard Deviations of the Distance Parameters of the Hydrogen Bridge in the Studied Molecules[a]

	HBZA		DMAP	
interatomic distance	average	SD	average	SD
O1−H2	1.053	0.085	1.018	0.031
O1...N3	2.601	0.108	2.769	0.178
H2...N3	1.641	0.162	1.857	0.223

[a] Results of the CPMD simulation. All values are in Å.

III. Results and Discussion

The models of the investigated Schiff (N-methyl-2-hydroxybenzylidene amine, HBZA) and Mannich (*ortho*-dimethylaminomethylphenol, DMAP) bases are presented in Figure 1. Car−Parrinello molecular dynamics simulations were performed in vacuo using the conditions applied during the experimental measurements of infrared (IR) spectra. Therefore, the correctness of the applied theoretical protocols was verified by comparison with the experimental data reported previously in the literature.[37,9] The features of the vibrational spectra are sensitive measures of the dynamic processes in the studied systems, and our attention will be concentrated on the properties of the intramolecular hydrogen bridge. Previous calculations for the compounds HBZA and DMAP performed on the basis of Density Functional Theory (DFT) and Møller-Plesset (MP2) perturbation theory[37,9] described the molecular properties based on static models; therefore, information on the intramolecular hydrogen bridge dynamics was not investigated. Our current study will discuss the results obtained on the basis of ab initio (CPMD) and path integral (PIMD) molecular dynamics and postprocessing analysis of the obtained trajectories.

The vibrational properties are direct derivatives of the time evolution of the structural parameters of the studied molecules. Therefore, the interatomic distances of the atoms involved in the intramolecular hydrogen bond were analyzed at the beginning of our study. The average values of the distance parameters of the hydrogen bridge are presented in Table 1 together with their standard deviations (SD). Increased SD might indicate delocalization events during the CPMD run. This might be suspected for the gas-phase simulation of HBZA, where not only the O−H bond length is longer than in DMAP but also the corresponding SD is almost three times larger. Accordingly, the donor−acceptor distance is shorter in HBZA and exhibits a smaller SD. This means that the intramolecular hydrogen bond of HBZA is stronger than that of DMAP. More details of the phenomena occurring in the analyzed bridges will be revealed in the time-domain analysis. The graphical representation of the obtained distances as a function of simulation time is presented in Figure 2. The main difference between the graphs for the investigated Schiff and Mannich bases is the presence of the bridged proton-transfer event after 3.5 ps of simulation time.

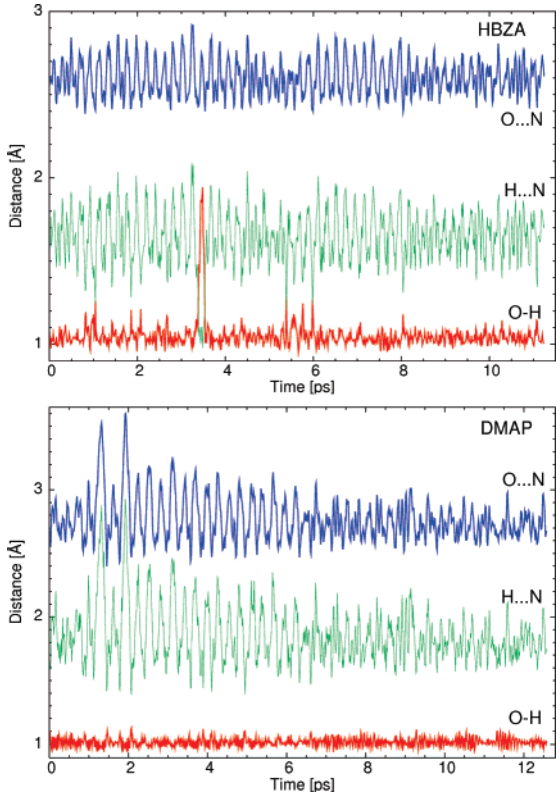

Figure 2. Time evolution of interatomic distances of atoms involved in the hydrogen bridge as a result of ab initio molecular dynamics.

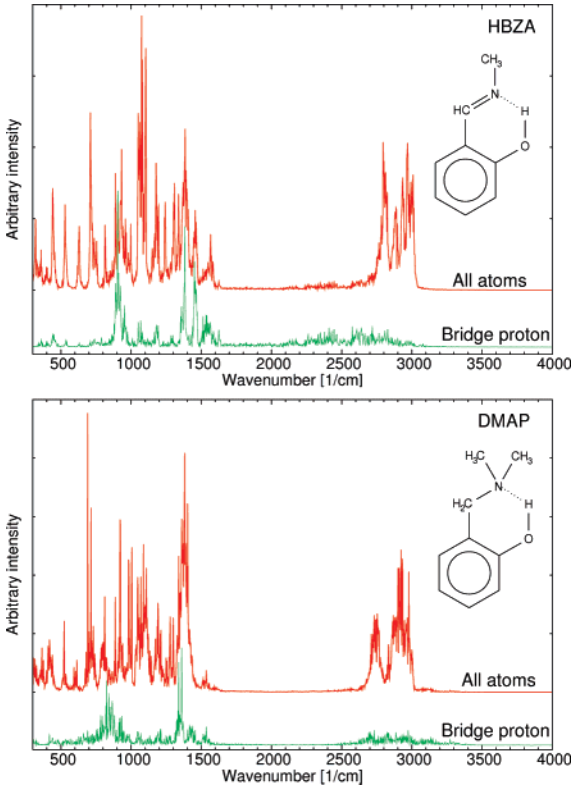

Figure 3. Power spectra of atomic velocities of all atoms and the hydrogen bridge proton. The intensities are in arbitrary units, while the wave numbers correspond to the actual vibrational features of the system.

Additionally, a few instances of equal donor−proton and acceptor−proton bond lengths are also visible which do not develop into full proton transfer. We have to stress that the transfer is not a permanent event but lasts only for ca. 0.2 ps, after which the proton returns to the donor site. In the case of the Mannich base, proton-transfer phenomena are not observed. The bridged proton remains totally at the oxygen atom, and the donor−proton distance is always significantly shorter than the proton−acceptor separation. This reflects the fact that the proton potential barrier is higher in DMAP than in HBZA, and it quite possibly has only one minimum at the donor site.

The atomic velocity power spectra generated from the CPMD trajectory of the investigated compounds are presented in Figure 3. In agreement with the discussion presented above, the spectra indicate various extents of proton delocalization in both molecules. The Schiff base HBZA is characterized experimentally by a very intense and broad absorption ascribed to the O−H stretching mode strongly coupled with other vibrational modes of the system.[37] The experimental data were collected in the gas phase at 300 K;[37] therefore, this is an internal property of the HBZA molecule, i.e., not induced or modified by environmental effects. Our calculations reflect this feature: the atomic velocity power spectrum for the bridged proton is almost continuous, with the high-frequency 2000−3000 cm^{-1} range corresponding to the O−H stretching mode. However, the gap between the low end of this band and the high end of the low-frequency proton modes is only 400 cm^{-1}. The experimentally available low-frequency part of the vibrational spectrum indeed shows bands at 1405, 1457, 1494, and 1639−1648 cm^{-1} which might correspond to our computational power spectra and which belong to modes coupled with bridge motions. The greater localization of the proton position in the dynamics of DMAP is related to the narrower proton absorption range (2550−3300 cm^{-1}) and the much larger separation from the low-frequency motions, which are present up to 1600 cm^{-1}. The experimental range attributed to the O−H stretching mode of DMAP's hydrogen bridge[9] is 2600−3450 cm^{-1}, centered at 3030 cm^{-1}. Our observations are strengthened by the dipole moment power spectra (Figure 3), which provide correct absorption intensities and are thus able to show the spectral effects of the hydrogen bond formation. In the case of HBZA, the calculated IR spectrum exhibits a broad region of absorption in the 2000−3000 cm^{-1} range. This feature does not appear in DMAP, a Mannich base with a markedly weaker intramolecular hydrogen bond. Concluding, we observed that our computational spectra are red-shifted with respect to the experimental data. For example, the maximum peak of the low-frequency region for HBZA is found experimentally[37] at 1639−1648 cm^{-1}, while our calculated value is 1580−1590 cm^{-1}. This red shift is a combined result of the use of the PBE functional within the framework of the DFT theory and application of Car−Parrinello dynamics, in which the fictitious mass used to propagate the electronic degrees of freedom introduces a delaying effect.

Path Integral Molecular Dynamics (PIMD) was applied to investigate the influence of quantum effects on proton delocalization. High computational overhead of the PIMD scheme restricted the number of Trotter replicas in our study

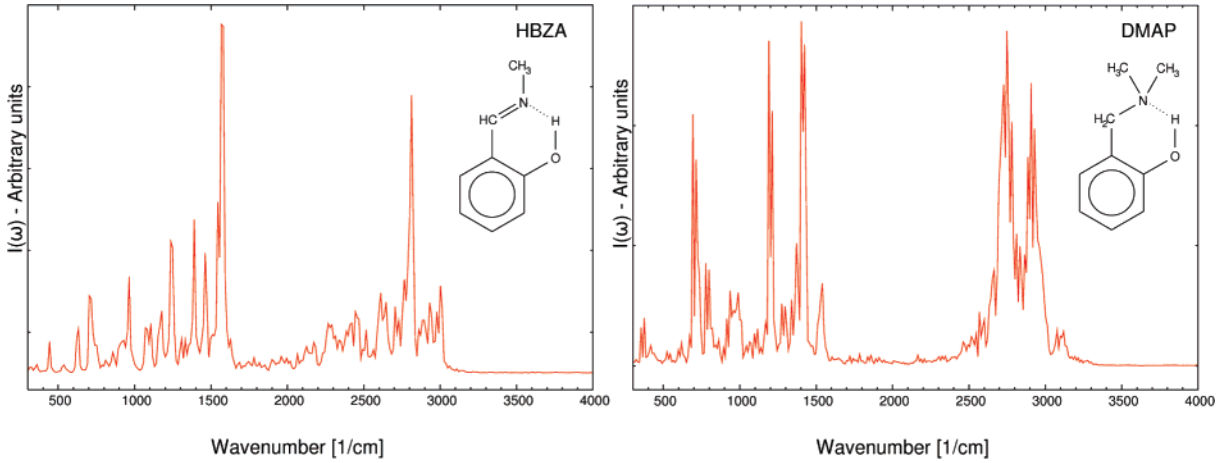

Figure 4. Predicted infrared spectra of studied Schiff and Mannich bases as results of ab initio molecular dynamics.

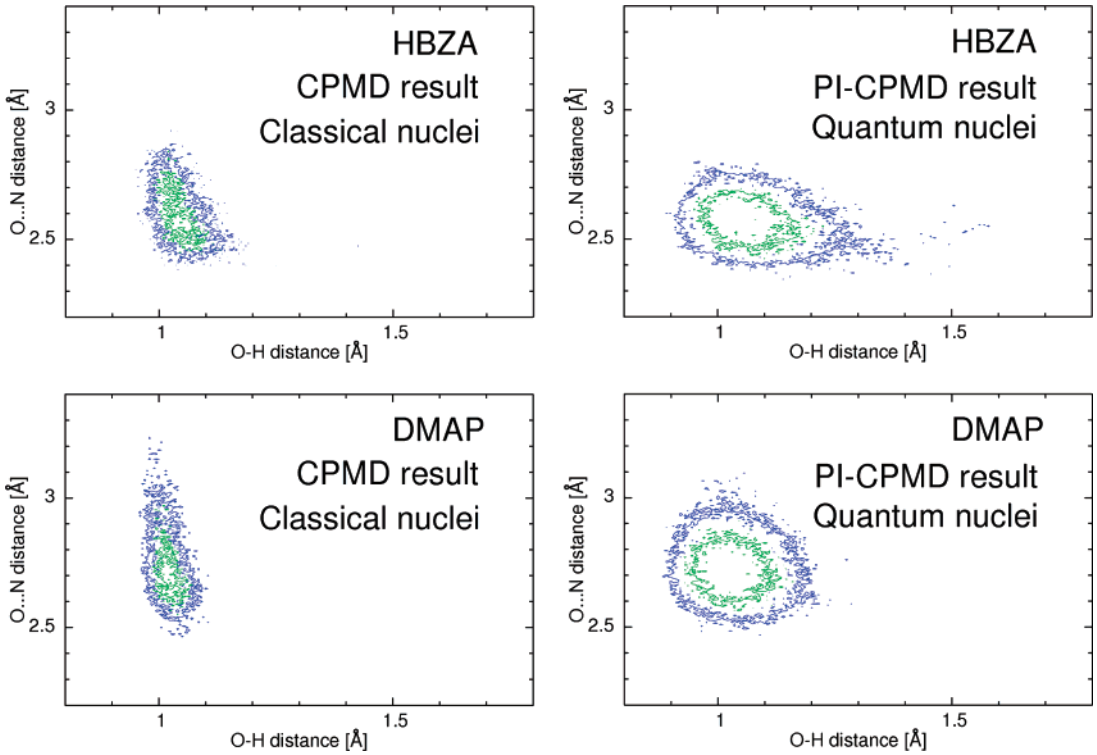

Figure 5. Comparison of the proton position in the hydrogen bridge reproduced by classical CPMD simulations (left side) and with quantum inclusion using the path integral (PI) method (right side) of studied Schiff (top) and Mannich (bottom) bases. The probability density isolines are 5 $Å^{-2}$ for the blue line and 15 $Å^{-2}$ for the green line.

to $P = 8$. Values of P as high as 16 were used to obtain converged potentials of mean force for model proton-transfer systems; the best example is a PIMD study on malonaldehyde.[61] However, the calculation of the pmf (described later in the text) proceeds in our case not from PIMD results but from a posteriori quantum corrections to the CPMD trajectory for the bridge proton. In view of the possible limitations of the convergence of the PIMD-derived pmf, we choose to discuss the effect of the quantization on the geometrical parameters only. Values of primitive[62] and virial[63] energy estimators provide an additional test of the PIMD convergence in terms of both simulation length and number of replicas. The PIMD run for HBZA yields the value of 0.06874 ± 0.01127 au for the primitive estimator and 0.06873 ± 0.00490 au for the virial expression. Corresponding run-averaged values and their standard deviations for the DMAP simulation are 0.09885 ± 0.01811 au (primitive estimator) and 0.09796 ± 0.00530 au (virial estimator), respectively. The agreement of average values of both estimators within a particular simulation suggests that the adopted calculation protocol provides reasonably converged results. Additionally, the standard deviations for the virial energy estimator are, correctly, smaller than for the primitive formula.[64] The tests described above enabled us to proceed with further analysis of the PIMD simulation. The two-dimensional (2D) histograms obtained for HBZA and DMAP are presented in Figure 5. A comparison of the results obtained on the basis of CPMD simulation (classical description of the nuclei) with PIMD is given in this chart. The two chosen coordinates, i.e., donor−acceptor distance and

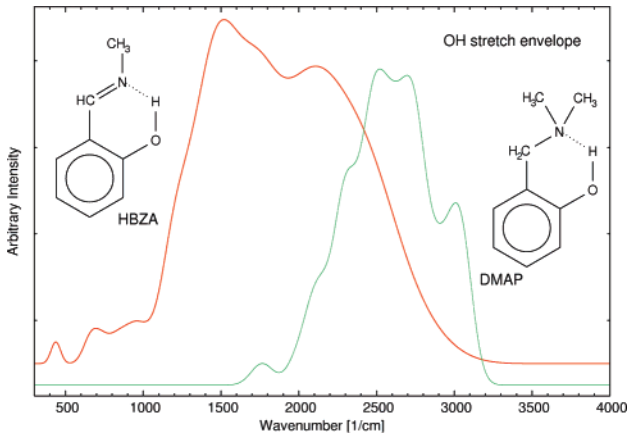

Figure 6. Simulated hydrogen bridge O−H stretching envelope in gas phase (arbitrary intensities on the Y axis) of the studied Schiff and Mannich bases.

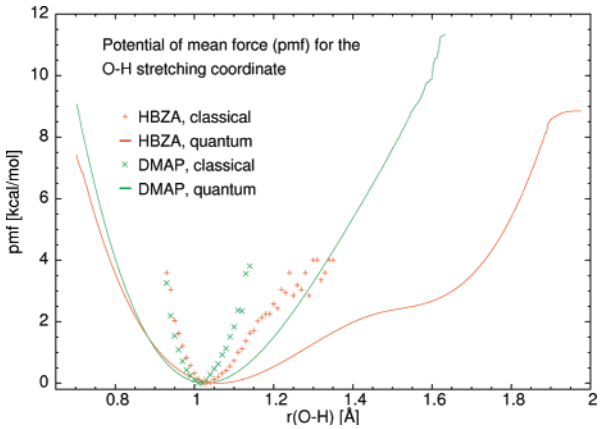

Figure 7. One-dimensional potential of mean force (1D pmf) for the O−H stretching mode calculated on the basis of CPMD simulation of the studied Schiff and Mannich bases. Markers denote the pmf resulting from classical nuclear probability density, while the solid lines are pmf curves augmented with quantization of nuclear motions.

O−H bond length, provide the most important characteristics of the investigated intramolecular hydrogen bond. Quantum effects seem to have a significantly stronger influence on the proton dynamics in HBZA compared with the DMAP molecule. The provided data analysis indicates the qualitative change in the proton's position (stronger delocalization) in the Schiff base. On the other hand, the classical CPMD description of the Mannich base does not exhibit significant differences from the PIMD histogram. The probability of proton transfer is higher at shorter donor−acceptor distances. It is worth mentioning that even the additional kinetic energy introduced by the higher simulation temperature (in the case of the Mannich base) was not able to promote proton transfer within the time frame of the simulation. Detailed analysis of Figure 5 reveals that the inclusion of quantum effects in the nuclear dynamics affects not only the proton's position but also the bridge as a whole. For HBZA, the histogram for donor−acceptor distances covers the range of 2.40−2.85 Å in the CPMD simulation, which shortens slightly to 2.40−2.80 Å when the PIMD technique is used. A similarly small shortening of the bridge due to quantum effects is also visible in DMAP, where the corresponding ranges are 2.50−3.05 Å for CPMD and 2.50−3.00 Å for PIMD. The respective values of the O−H distances indicate increased proton delocalization in PIMD, as mentioned above. In HBZA, the O−H bond lengths range from 0.98−1.15 Å for classical nuclei to 0.92−1.35 Å in the PIMD simulation. In the latter case there are also isolated instances of much larger O−H separations, corresponding to instantaneous proton-transfer events. DMAP does not display such a behavior, but the accessible O−H distance range increases from 0.98−1.10 Å in CPMD to 0.90−1.20 Å for quantized nuclear degrees of freedom. In summary, inclusion of a quantum description of the nuclei seems to affect the Mannich base to a smaller degree than the Schiff base and does not change the qualitative description of the hydrogen bridge in DMAP.

A posteriori inclusion of quantum effects of the proton motion provides us with the possibility of computing the spectral features corresponding to the proton motion in the bridge (Figure 6) and the one-dimensional potential of mean force (1D pmf) for the O−H coordinate (Figure 7). Figure 6 shows that for DMAP the calculated spectral feature corresponds to the O−H stretching region, while for the stronger intramolecular hydrogen bond the coupling between various modes broadens the feature toward the low-frequency part of the spectrum. This leads to the formation of an almost continuous, very broad band. Comparison with Figure 3, where classical power spectrum is presented, shows that the broadening is a result of quantum corrections allowing the proton to probe larger range of positions, where anharmonicity is pronounced much stronger. This is more important for the HBZA with its stronger hydrogen bond, than for DMAP. The corresponding 1D pmf for the O−H coordinate (Figure 7) reflects this difference in the proton dynamics. Most significantly, the classical pmf calculated directly from the O−H probability distribution of the CPMD run is more localized than the result of a posteriori quantum corrections. The difference between HBZA and DMAP proton dynamics is visible even in the classical pmf. However, it suffers from inadequate statistical sampling above 3.0 kcal/mol (oscillations in Figure 7), and further we discuss only the quantum-corrected results. While for DMAP the potential is anharmonic but similar to the Morse potential, the HBZA molecule has a very asymmetric 1D pmf with a distinct shoulder related to possible instantaneous proton-transfer events. The minimum of the 1D pmf for DMAP (containing quantum effects) corresponds to the average O−H distance from the classical-nuclei CPMD simulation (Table 1), confirming the PIMD result stating that the quantization of proton motion does not have a strong impact on the ensemble averages in the case of the Mannich base. The 1D pmf minimum is shifted to a larger O−H bond length value (ca. 1.07 Å) for HBZA, but the difference from the classical simulation is visible rather in the flattening of the potential.

A more detailed overview of the proton dynamics in the hydrogen bridge is provided by the graphs of the two-dimensional potential of mean force (2D pmf) for both compounds (Figure 8). The choice of the analyzed coordinates, the O−H distance and O−H...N angle, was dictated by their structural relevance to proton mobility. We decided not to discuss the motion of the heavy atoms involved in

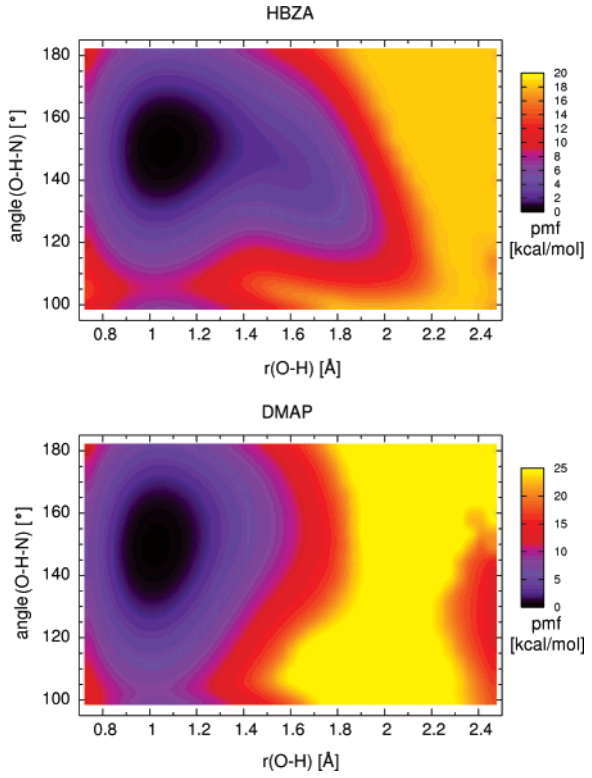

Figure 8. Two-dimensional potential of mean force (2D pmf) for the O−H stretching mode calculated on the basis of CPMD simulation augmented by quantization of nuclear motions. Upper graph: results for the Schiff base, lower graph: for the Mannich base.

the hydrogen bridge, i.e., the O...N distance is not a coordinate chosen for the graph. Instead, the graph provides a statistically averaged potential for the proton motion "as seen by the proton" and defined by the coordinates directly involving this nucleus. The 2D pmf map for HBZA exhibits a potential well centered at r(O−H) equal to 1.05 Å and an O−H...N angle equal to 150°. The same parameters are found for the Mannich base. However, a second, very shallow minimum of the pmf is present in HBZA but not in DMAP. The coordinates of this feature are r(O−H) = 1.60 Å and an O−H...N angle of 140°. This secondary minimum corresponds to instantaneous proton-transfer phenomena, which are more probable within a quantized proton-motion framework. The picture obtained by investigation of the 2D free energy profile is totally consistent with the PIMD results for both compounds.

The methodology of calculation of the pmf by a posteriori quantum corrections to the CPMD trajectory snapshots, used previously in 1D case[55] and extended here to a 2D problem, is an addition to the large set of schemes for free energy computation. Methods such as replica exchange molecular dynamics[65] can provide rapid access to the complicated conformational space of macromolecules, describing, e.g., the process of reversible protein folding.[66] Constrained molecular dynamics[67] also provides a convenient route for obtaining free energy profiles directly from the MD simulation. Additionally, in the low-dimensional case there exist numerous enhanced sampling methods, a few of which are discussed below. Umbrella sampling, in its native[68,69] or semiautomated, adaptative version,[70] modifies the potential energy surface (PES) of the system to overcome locality of standard Boltzmann sampling. Metadynamics[71] modifies the PES with history-dependent potential terms which fill up the PES minima allowing for further recovery of rare-event statistics, which is especially useful in the context of first-principle molecular dynamics.[72] Finally, adiabatic free energy dynamics[73] separates reaction coordinate subspace from the rest of the phase space and enhances probability of rare events by applying large temperature to the reaction subspace only. The methodologies described above are general and applicable to any reaction coordinate. Moreover, they can be implemented within classical MD, first-principle MD, or path integral nuclear quantization schemes. The pmf calculation method of the current paper is, in principle, restricted to the description of localized vibrational coordinates. It is intended as a relatively inexpensive way of further analysis of a classical-nuclei CPMD trajectory, providing at the same time pmf profile and spectral signature of a selected coordinate. Therefore, this method can be advantageous in studies emphasizing important local interactions, especially intra- or intermolecular hydrogen bonds.

IV. Conclusions

Our computational investigations showed that the applied methodologies were able to describe faithfully the molecular properties of the studied Schiff and Mannich bases. Car−Parrinello molecular dynamics augmented by a posteriori quantum corrections is particularly valuable in studies of hydrogen bridge dynamics. The application of path integral molecular dynamics showed that in the case of the bridged proton of the studied Schiff base, the quantum effects improve the description of the proton's position in the intramolecular hydrogen bond and enable the possibility of proton transfer. The bridged proton position is localized on the donor side in the Mannich base. The vibrational properties were also analyzed, and they are closely related to the available experimental measures of proton delocalization. The one- and two-dimensional free energy profiles were obtained from the eigenfunctions of the vibrational states of the studied molecules. The resulting potential of mean force for the proton motion describes the proton-transfer pathway, which includes quantum corrections to the classical picture. In the case of the Schiff base, proton transfer can occur with a quite large probability, while in the Mannich base the proton is mostly localized on the donor side. The computational strategy employed in the study has shown its potential for describing the influence of structural modifications of the molecular skeleton on the properties of the O−H...N hydrogen bridge. We are currently extending the use of the methodology to other strongly anharmonic systems. The proposed 2D pmf technique could be applied to study the free energy profiles of large systems with biological relevance, especially when coupled with the QM/MM simulation framework.

Acknowledgment. The authors would like to thank Dr. Sonia M. Melikova (University of St. Petersburg), Dr. Riccardo Mazzarello (SISSA, Trieste), and Prof. Aleksander

Koll (University of Wrocław) for fruitful discussions and critical reading of the manuscript and Dr. Harald Forbert (Ruhr-Universität Bochum) for the program for dipole moment Fourier transforms. In addition, the authors gratefully acknowledge the Wrocław Center for Networking and Supercomputing (WCSS), the Academic Computer Center CYFRONET-KRAKÓW (grants KBN/SGI/UWrocl/029/1998 and KBN/SGI/UWrocl/078/2001), and the Poznań Supercomputing and Networking Center for providing computer time and facilities.

References

(1) Warshel, A. *Computer Modelling of Chemical Reactions in Enzymes and Solutions*, 1st ed.; Wiley: New York, NY, 1997; pp 136−152.

(2) Jeffrey, G. A. *An Introduction to Hydrogen Bonding*, 1st ed.; Oxford University Press: New York, NY, 1997; pp 184−212.

(3) Cleland, W. W.; Kreevoy, M. M. *Science* **1994**, *264*, 1887−1890.

(4) Gao, J.; Truhlar, D. G. *Annu. Rev. Phys. Chem.* **2002**, *53*, 467−505.

(5) Denisov, G. S.; Mavri, J.; Sobczyk, L. Potential energy shape for the proton motion in hydrogen bonds reflected in infrared and NMR spectra. In *Hydrogen bonding - new insights*, *(Challenges and advances in computational chemistry and physics*, *3*), 1st ed.; Grabowski, S. J., Ed.; Springer: Dordrecht, The Netherlands, 2006; pp 377−416.

(6) Zundel, G. Hydrogen-bonded systems with large proton polarizability due to collective proton motion as pathways of protons in biological systems. In Müller, A.; Ratajczak, H.; Junge, W.; Diemann, E. *Electron and Proton Transfer in Chemistry and Biology*; Elsevier: Amsterdam, The Netherlands, 1992; pp 313−327.

(7) Król-Starzomska, I.; Filarowski, A.; Rospenk, M.; Koll, A.; Melikova, S. *J. Phys. Chem. A* **2004**, *108*, 2131−2138.

(8) Filarowski, A. *J. Phys. Org. Chem.* **2005**, *18*, 686−698.

(9) Koll, A.; Melikova, S. M.; Karpfen, A.; Wolschann, P. *J. Mol. Struct.* **2001**, *559*, 127−145.

(10) Filarowski, A.; Koll, A.; Głowiak, T. *J. Chem. Soc. Perkin Trans.* **2002**, *2*, 835−842.

(11) Filarowski, A.; Głowiak, T.; Koll, A. *J. Mol. Struct.* **1999**, *484*, 75−89.

(12) Rospenk, M.; Król-Starzomska, I.; Filarowski, A.; Koll, A. *Chem. Phys.* **2003**, *287*, 113−124.

(13) Filarowski, A.; Koll, A.; Głowiak, T. *J. Mol. Struct.* **2002**, *615*, 97−108.

(14) Filarowski, A.; Koll, A. *Vib. Spectrosc.* **1996**, *12*, 15−24.

(15) Schilf, W.; Kamiński, B.; Kołodziej, B.; Grech, E.; Rozwadowski, Z.; Dziembowska, T. *J. Mol. Struct.* **2002**, *615*, 141−146.

(16) Washington, I.; Brooks, C.; Turro, N. J.; Nakanishi, K. *J. Am. Chem. Soc.* **2004**, *126*, 9892−9893.

(17) Shimono, K.; Furutani, Y.; Kamo, N.; Kandori, H. *Biochemistry* **2003**, *42*, 7801−7806.

(18) Maeda, A.; Gennis, R. B.; Balashov, S. P.; Ebrey, T. G. *Biochemistry* **2005**, *44*, 5960−5968.

(19) Furutani, Y.; Shichida, Y.; Kandori, H. *Biochemistry* **2003**, *42*, 9619−9625.

(20) Tanimoto, T.; Furutani, Y.; Kandori, H. *Biochemistry* **2003**, *42*, 2300−2306.

(21) Lee, Y-S.; Krauss, M. *J. Am. Chem. Soc.* **2004**, *126*, 2225−2230.

(22) Hadjoudis, E.; Vittorakis, M.; Moustakali-Mavridis, I. *Tetrahedron* **1987**, *43*, 1345−1360.

(23) Harada, J.; Uekusa, H.; Ohashi, Y. *J. Am. Chem. Soc.* **1999**, *121*, 5809−5810.

(24) Evans, O. R.; Lin, W. *Acc. Chem. Res.* **2002**, *35*, 511−522.

(25) Toftlund, H. *Coord. Chem. Rev.* **1989**, *94*, 67−108.

(26) León-Clemente, M.; Coronado, E.; Delhaes, P.; Galán Mascarós, J. R.: Gómez-García, C. J.; Mingotaud, C. Hybrid materials formed by two molecular networks. Magnetic conductors, magnetic multilayers and magnetic films. In *Supramolecular Engineering of Synthetic Metallic Materials: Conductors and Magnets*, *NATO ASI Series*; Veciana, J., Rovira, C., Amabilino, D. B., Eds.; Kluwer: Dordrecht, The Netherlands, 1998; Vol. C-518, pp 291−312.

(27) Vashishtha, S. C.; Zello, G. A.; Nienaber, K. H.; Balzarini, J.; De Clercq, E.; Stables, J. P.; Dimmock, J. R. *Eur. J. Med. Chem.* **2004**, *39*, 27−35.

(28) Holla, B. S.; Veerendra, B.; Shivananda, M. K.; Poojary, B. *Eur. J. Med. Chem.* **2003**, *38*, 759−767.

(29) Malinka, W.; Karczmarzyk, Z.; Sieklucka-Dziuba, M.; Sadowski, M.; Kleinrok, Z. *Il Farmaco* **2001**, *56*, 905−918.

(30) Sridhar, S. K.; Saravanan, M.; Ramesh, A. *Eur. J. Med. Chem.* **2001**, *36*, 615−625.

(31) Sriram, D.; Bal, T. R.; Yogeeswari, P. *Med. Chem. Res.* **2005**, *14*, 211−228.

(32) Goldstein, E. J. *Am. J. Med.* **1987**, *82*, 3−17.

(33) Pandeya, S. N.; Sriram, D.; Nath, G.; De Clercq, E. *Eur. J. Med. Chem.* **2000**, *35*, 249−255.

(34) Pandeya, S. N.; Sriram, D.; Yogeeswari, P.; Ananthan, S. *Chemotherapy* **2001**, *47*, 266−269.

(35) Kleist, R. A.; Gutierrez, A.; Lundberg, R. D.; Song, W. R. U.S. Patent No. 5,433,874 (July 18, 1995).

(36) Air Products and Chemicals, Inc., U.S. Patent No. 5,854,-312 (December 29, 1998).

(37) Filarowski, A.; Koll, A.; Karpfen, A.; Wolschann, P. *Chem. Phys.* **2004**, *297*, 323−332.

(38) Car, R.; Parrinello, M. *Phys. Rev. Lett.* **1985**, *55*, 2471−2474.

(39) Hohenberg, P.; Kohn, W. *Phys. Rev.* **1964**, *136*, B864−B871.

(40) Kohn, W.; Sham, L. J. *Phys. Rev.* **1965**, *140*, A1133−A1138.

(41) Kirkwood, J. G. *J. Chem. Phys*. **1935**, *3*, 300−313.

(42) Schlegel, H. B. *Theor. Chim. Acta* **1984**, *66*, 333−340.

(43) Perdew, J. P.; Burke, K.; Ernzerhof, M. *Phys. Rev. Lett.* **1996**, *77*, 3865−3868.

(44) Troullier, N.; Martins, J. L. *Phys. Rev. B* **1991**, *43*, 1993−2006.

(45) Marx, D.; Parrinello, M. *Science* **1996**, *271*, 179−181.

(46) Marx, D.; Parrinello, M. *J. Chem. Phys.* **1996**, *104*, 4077−4082.

(47) Tuckerman, M. E.; Marx, D.; Klein, M. L.; Parrinello, M. *J. Chem. Phys.* **1996**, *104*, 5579−5588.

(48) Nosé, S. *Mol. Phys.* **1984**, *52*, 255−268.

(49) Nosé, S. *J. Chem. Phys.* **1984**, *81*, 511−519.

(50) Hoover, W. G. *Phys. Rev. A* **1985**, *31*, 1695−1697.

(51) Martyna, G. J.; Klein, M. L.; Tuckerman, M. E. *J. Chem. Phys.* **1992**, *97*, 2635−2643.

(52) Tuckerman, M. E.; Berne, B. J.; Martyna, G. J.; Klein, M. L. *J. Chem. Phys.* **1993**, *99*, 2796−2808.

(53) Stare, J.; Mavri, J. *Comput. Phys. Commun.* **2002**, *143*, 222−240.

(54) Panek, J.; Stare, J.; Hadži, D. *J. Phys. Chem. A* **2004**, *108*, 7417−7423.

(55) Jezierska, A.; Panek, J. J.; Koll, A.; Mavri, J. *J. Chem. Phys.* **2007**, *126*, 205101.

(56) Jezierska, A.; Panek, J. J.; Borštnik, U.; Mavri, J.; Janežič, D. *J. Phys. Chem. B* **2007**, *111*, 5243−5248.

(57) CPMD, Copyright IBM Corp. 1990−2004, Copyright MPI fuer Festkoerperforschung Stuttgart, 1997−2001.

(58) Ventura, K. M.; Greene, S. N.; Halkides, C. J.; Messina, M. *Struct. Chem.* **2001**, *12*, 23−31.

(59) Humphrey, W.; Dalke, A.; Schulten, K. *J. Mol. Graph.* **1996**, *14*, 33−38.

(60) Williams, T.; Colin, K. Copyright 1986−1993, 1998, 2004.

(61) Tuckerman, M. E.; Marx, D. *Phys. Rev. Lett.* **2001**, *86*, 4946−4949.

(62) Barker, J. A. *J. Chem. Phys.* **1979**, *70*, 2914−2918.

(63) Herman, M. F.; Bruskin, E. J.; Berne, B. J. *J. Chem. Phys.* **1982**, *76*, 5150−5155.

(64) Parrinello, M.; Rahman, *J. Chem. Phys.* **1984**, *80*, 860−867.

(65) Mitsutake, A.; Sugita, Y.; Okamoto, Y. *Biopolym. Pept. Sci.* **2001**, *60*, 96−123.

(66) Rao, F.; Caflisch, A. *J. Chem. Phys.* **2003**, *119*, 4035−4042.

(67) Sprik, M.; Ciccotti, G. *J. Chem. Phys.* **1998**, *109*, 7737−7744.

(68) Patey, G. N.; Valleau, J. *J. Chem. Phys.* **1975**, *63*, 2334−2339.

(69) Torrie, G.; Valleau, J. P. *J. Comput. Phys.* **1977**, *23*, 187−199.

(70) Mezei, M. *J. Comput. Phys.* **1987**, *68*, 237−240.

(71) Laio, A.; Parrinello, M. *Proc. Natl. Acad. Sci. U.S.A.* **2002**, *99*, 12562−12566.

(72) Asciutto, E.; Sagui, C. *J. Phys. Chem. A* **2005**, *109*, 7682−7687.

(73) Rosso, L.; Tuckerman, M. E. *Mol. Simul.* **2002**, *28*, 91−112.

CT7002644